Petroleum Science 20 (2023) 879–892

Contents lists available at ScienceDirect

Petroleum Science

journal homepage: www.keaipublishing.com/en/journals/petroleum-science

Original Paper

Well logging evaluation of fine-grained hydrate-bearing sediment reservoirs: Considering the effect of clay content

Lin-Qi Zhu [a, b, c], Jin Sun [a, c], Xue-Qing Zhou [a, c], Qing-Ping Li [d, e], Qi Fan [d, e], Song-Lin Wu [a], Shi-Guo Wu [a, b, c, *]

[a] Laboratory of Marine Geophysics and Georesources of Hainan Province, Institute of Deep-sea Science and Engineering, Chinese Academy of Sciences, Sanya, 572000, Hainan, China
[b] Laboratory for Marine Geology, Qingdao National Laboratory for Marine Science and Technology, Qingdao, 266061, Shandong, China
[c] Southern Marine Science and Engineering Guangdong Laboratory (Zhuhai), Zhuhai, Guangdong, 519000, China
[d] State Key Laboratory of Natural Gas Hydrates, Beijing, 100028, China
[e] China National Offshore Oil Corporation Research Institute Co. Ltd., Beijing, 100028, China

ARTICLE INFO

Article history:
Received 10 January 2022
Received in revised form
21 July 2022
Accepted 16 September 2022
Available online 21 September 2022

Edited by Jie Hao

Keywords:
Gas hydrate
Well logging
Porosity
Saturation
Shale distribution form

ABSTRACT

Hydrate reservoirs are different from the host reservoirs of all other fossil energy sources because the characteristics of hydrate reservoirs are generally controlled by deep-sea fine-grained sedimentation. In such reservoirs, the reliability of the classical logging evaluation models established for diagenetic reservoirs is questionable. This study used well W8 in the Qiongdongnan Basin to explore the clay content, porosity, saturation, and hydrate-enriched layer identification of a logging-based hydrate reservoir, and it was found that considering the effect of the clay content on the log response is necessary in the logging evaluation of hydrate reservoirs. In the evaluation of clay content, a method based on the optimization inversion method can obtain a more reliable clay content than other methods. Fine-grained sediment reservoirs have a high clay content, and the effect of clay on log responses must be considered when calculating porosity. In addition, combining density logging and neutron porosity logging data can obtain the best porosity calculation results, and the porosity calculation method based on sonic logging predicted that the porosity of the studied reservoir was low. It was very effective to identify hydrate layers based on resistivity, but the clay distribution and pore structure will also affect the relationship between resistivity, porosity and saturation, and it was suggested that the factors effecting the resistivity of different layers should be considered in the saturation evaluation and that a suitable model should be selected. This study also considered the lack of clarity of the relationships among the lithology, physical properties, hydrate-bearing occurrence properties, and log response properties of hydrate reservoirs and the lack of specialized petrophysical models. This research can directly help to improve hydrate logging evaluation.

1. Introduction

Natural gas hydrate is a fossil energy formed by water and natural gas molecules under relatively high-pressure and low-temperature conditions (Collett, 1993; Cook et al., 2020; Wang et al., 2021a). It is a special form of natural gas that exists in nature and is mainly distributed below the seabed in deep water (usually greater than 300 m) and in the permafrost zone. Deep-sea gas hydrates usually occur in the gas hydrate stability zone (GHSZ), and the bottom boundary of the stability zone is often determined by the bottom simulating reflector (BSR) of processed seismic data (Horozal et al., 2017; Portnov et al., 2019; Gullapalli et al., 2019; Yang et al., 2020; Han et al., 2021). Since the formation of natural gas hydrate requires the temperature of the reservoir to be low, the water depth of the reservoir is usually deep. In this case, among the deep-sea fine-grained sediments usually host a large amount of hydrates when the gas source is sufficient (Jang et al., 2020; Zhou

* Corresponding author. Laboratory of Marine Geophysics and Georesources of Hainan Province, Institute of Deep-sea Science and Engineering, Chinese Academy of Sciences, Sanya, 572000, Hainan, China.
E-mail address: swu@idsse.ac.cn (S.-G. Wu).

https://doi.org/10.1016/j.petsci.2022.09.018

et al., 2021; Li et al., 2021). Considering the amount of methane in natural gas hydrates, natural gas hydrates are regarded as a resource or part of the global carbon cycle and have aroused interest. The United States, China, India and other countries have formulated natural gas hydrate exploration and development plans (Kret et al., 2020; Qi et al., 2022; Singh and Ojha, 2022; Zhu et al., 2022b).

Considering the heterogeneity of hydrate distribution in a formation and the resolution of seismic technology, even if the GHSZ can be qualitatively identified by seismic methods, the quantitative identification of hydrate occurrence in the GHSZ is still unclear (Pandey et al., 2019; Saito et al., 2019; Waite et al., 2019; Ghosh and Ojha, 2021). Drilling and coring analysis of a whole well section is an effective method to clarify the fine distribution of hydrates, but it is difficult because hydrate deposits tend to change during coring (Wu et al., 2016; Kato et al., 2019; Hu et al., 2021; Singh et al., 2022). Moreover, with the development of hydrates, the efficiency of coring and experimenting throughout the well section is too low.

Well logging can measure the acoustic, electrical, nuclear physics and other physical properties of the formation near the drilled borehole and calculate reservoir parameters through these physical properties (Shankar et al., 2013; Cheng et al., 2017; Lin et al., 2022). Currently, logging can be performed along the entire well section, and coring experiments can be conducted in key formations. This is an effective method to reduce core recovery efforts and improve the efficiency of exploration and development (Jain et al., 2019; Shaibu et al., 2021; Zhu et al., 2021, 2022a). Logging curves and corresponding petrophysical models can be used to obtain the reservoir parameter change characteristics over the entire GHSZ depth range and to achieve the refined exploration and development of hydrates (You et al., 2021; Zhong et al., 2021; Qian et al., 2018; Ghosh and Ojha, 2021). The interpretation accuracy of reservoir parameters based on logging methods depends on the measurement results and the rationality of the petrophysical model. In response, some researchers have conducted logging evaluation studies of hydrate reservoirs. Collett et al. (2011) used log and core data to evaluate formations at the Mount Elbert Gas Hydrate Stratigraphic Test Well, Alaska North Slope. Wang et al. (2011) combined sonic and resistivity logging to calculate the formation saturation in the Shenhu area, South China Sea. Yadav et al. (2019) used acoustic logging to estimate the amount of gas hydrate, considering both isotropic (pore-filling) and anisotropic (fracture-filling) acoustic reservoir models. Saumya et al. (2019) improved the full-wave train sampling interval length of acoustic logging to extract more reliable acoustic curves and improve the reliability of porosity prediction.

It is undeniable that senior researchers have conducted a considerable amount of research to obtain more appropriate and targeted petrophysical models of weak diagenetic hydrate reservoirs with deep-sea fine-grained sedimentary characteristics. For example, Sun et al. (2021) proposed an Archie saturation model based on digital cores. Qian et al. (2019) proposed an anisotropic saturation model for fracture-filled gas hydrate reservoirs. Pandey et al. (2019) proposed a calculation method of saturation based on longitudinal wave velocity and resistivity. Joshi conducted gas hydrate saturation evaluations at the NGHP-02-17 and NGHP-02-19 stations based on an anisotropic velocity model. Wang et al. (2021b) proposed a saturation evaluation model based on dielectric logging. Liu et al. (2020) derived a petrophysical model of the saturation and permeability of hydrate reservoirs based on fractal theory. Cai et al. (2020) analysed the creep of gas hydrate reservoirs and presented a fractal permeability model. However, the relevant research is primarily based on basic rock physics: reservoir petrophysical experiments need to be further developed to elucidate the spatiotemporal variations in this rock. This has led to the current log-based petrophysical models of hydrate reservoirs that are mostly appropriate for conventional diagenetic oil and gas reservoirs, which are very different from hydrate reservoirs, so the physical response of hydrate reservoirs with deep-sea sedimentary characteristics must be considered. As hydrate exploration continues, an increasing number of types of hydrate reservoirs have been discovered. For fine-grained hydrate reservoirs with stronger heterogeneity, such as leaking gas hydrate reservoirs, the difference in quality among reservoirs is greater, and the reliability of reservoir parameter calculations is even more critical. The accuracy of the petrophysical model is undoubtedly of growing concern.

The Qiongdongnan (QDN) Basin in the northern part of the South China Sea is an area rich in fossil energy (Wei, 2021). Under the tectonic geological background of the quasi passive continental margin, it has stable high-pressure and low-temperature conditions that allow the formation of natural gas hydrate. In this investigation, indirect evidence of the existence of natural gas hydrates, such as BSRs (Liang et al., 2019; Meng et al., 2021), cold springs (Fang et al., 2019), and geochemical anomalies, was discovered (Wei et al., 2021). In 2018, the Guangzhou Marine Geological Survey conducted gas hydrate drilling (GMGS5 expedition) on the Songnan Low Uplift in the eastern part of the QDN area (Ye et al., 2019; Wei and Deng, 2020). Various forms of hydrate, such as massive, layered, veined, and nodular hydrates, were found in cored boreholes on multiple gas chimneys, and conventional and specialized logging measurements were performed. Therefore, suitable data were made available for testing the effect of logging interpretation. Based on these data, this paper discusses the effect of the proposed petrophysical model under different assumptions on the evaluation of deep-sea fine-grained hydrate reservoirs with higher mud contents and proposes the development direction of hydrate reservoir logging evaluation.

2. Data

The research data were based on the GMGS5 expedition. The data were primarily related to well W8. All data were collected from publicly published documents and datasets.

The database used in this article includes a complete set of core data and the corresponding conventional logging data and nuclear magnetic resonance (NMR) logging porosity data. The core data originated from pressure-holding coring and conventional coring. This research first calculated the clay content, porosity, and saturation based on logging curves and different petrophysical models (although permeability is also a very important parameter, especially for development, the current permeability model is theoretically inconsistent with the known properties of hydrate reservoirs; in addition, specialized logging data, such as NMR logging data, were used to calculate permeability, which was difficult to obtain directly from the published literature) and then compared the results with public core data to discuss the effect and development direction of the model (Ge et al., 2017a, 2017b).

Logging data are implemented by Schlumberger Oilfield Services' Logging While Drilling (LWD) tools, specifically MicroScope, NeoScope, TeleScope, SonicScope, and ProVISION. With these LWD tools, natural gamma logging, calliper logging, density logging, neutron porosity logging, sonic logging, ring resistivity logging, shallow resistivity logging, medium depth resistivity logging, deep resistivity logging, and NMR logging data were obtained.

The clay content data were determined through particle size and lithology analysis experiments. Some core samples were used, but not necessarily pressure-holding core samples. There were two ways to determine saturation: one was to directly determine by the coring process maintaining pressure. Regardless of gas escape during operation, the saturation determined by this method should

be the most accurate. However, the cost is also the highest, and satisfactory results may not be obtained. Calculating saturation based on chloride ion concentration is also a way to provide reliable saturation results, even when the chloride ion concentration is not neutralized. Well W8 was the main well studied in this article because it had a large hydrate-containing layer. Taking well W8 (water depth 1737.4 m) as an example and assuming that chlorine was a conservative species, the hydrate concentration was calculated based on the degree of desalination of the pore water. From the bottom of the sea to 50.3 mbsf, the concentrations of chloride ions were all 630 mM, and as the depth of the formation continued to increase, the concentration of chloride ions began to change, and this change can be converted into the hydrate saturation. Fig. 1 shows the logging data and core data of well W8. These data were the basis of this article.

3. Methods

3.1. Clay content

In a logging-based reservoir evaluation program, clay content should be one of the core reservoir parameters, especially for fine-grained reservoirs. First, the clay content controls the quality of the reservoir. Because the particle size of clay is finer than that of silt sand (less than 0.01 mm), the increase in clay content will affect the quality of the reservoir, such as reducing the porosity. The increase in clay content will also block the pore throats, making sediment seepage more difficult and the sediment become less favourable as a hydrate host. Clay content also had an impact on the physical response of the formation because its properties are very different from coarse-grained quartz, feldspar, calcite, etc. Clay is radioactive, so it will affect the count rate of natural gamma logging. Clay contains bound water, crystal water, etc., and has a high hydrogen index. The density of clay is usually lower than that of quartz, which leads to a decrease in the density log response of the formation when the clay content is high. In addition, when the clay content is high, the resistivity of the formation will decrease significantly, and some types of clay will also produce cation exchange to enhance the conductivity of the skeleton. The accurate calculation of clay content was the first step in this work. Unfortunately, there have been few studies on the applicability of models for evaluating clay content in hydrate reservoirs.

The methods for calculating the clay content of conventional coarse-grained diagenetic reservoirs can be roughly attributed to statistical methods, log curve relative value methods, mineral composition inversion methods, intersection charts, resistivity methods, and evaluation methods based on machine learning.

As the data of hydrate reservoir wells are inherently scarce, the clay content evaluation method based on machine learning is difficult to use and is not further discussed here. The statistical method was used to find the correlation between the logging curve and clay content. Statistical methods include unit statistical methods and multivariate statistical methods. The relative value method of logging curves is a common calculation method. Spontaneous potential logging, natural gamma logging, and natural gamma spectroscopy logging data can be combined with the relative value method to calculate the clay content. Taking natural gamma logging data as an example, the most common calculation methods in conventional reservoirs are (Larinonv, 1969; Poupon and Gaymard, 1970):

$$I_c = \frac{GR - GR_{min}}{GR_{max} - GR_{min}} \tag{1}$$

$$V_c = \frac{2^{cI_c} - 1}{2^c - 1} \tag{2}$$

In the formula above, I_c refers to the relative value of the natural gamma curve, GR, GR_{min} and GR_{max} are the natural gamma log values of clay-bearing sediments, pure sandy sediments and pure

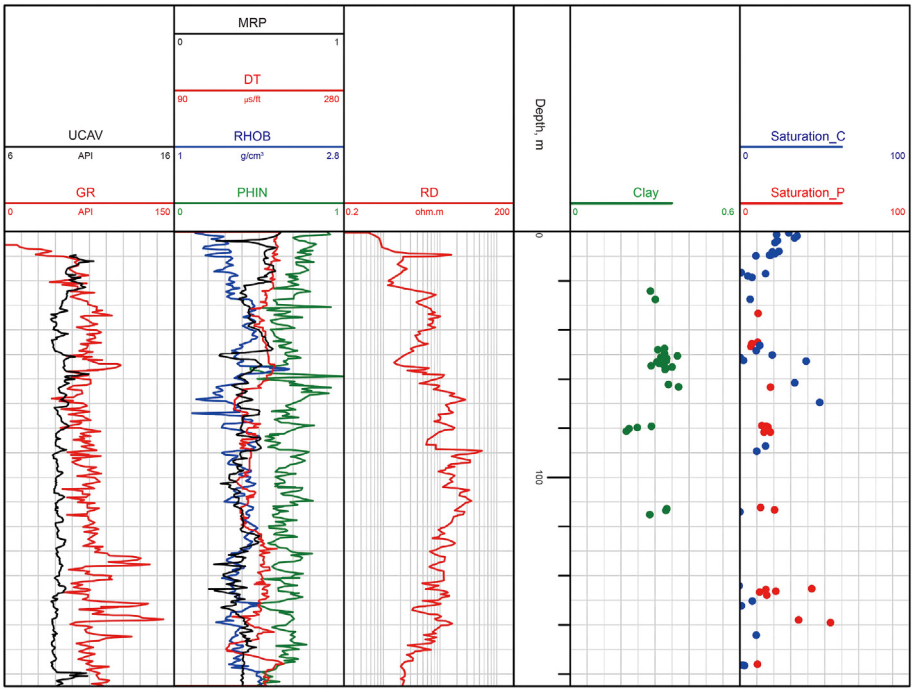

Fig. 1. Data from well W8 in the QDN area used in this article, where UCAV is the calliper log, GR is the natural gamma log, PHIN is the neutron porosity log, RHOB is the density log, DT is the sonic log, MRP is the NMR log porosity, and RD is the deep resistivity log. Clay is the core clay content, Saturation_C is the core hydrate saturation determined based on the salinity data of the formation water, and Saturation_P is the core hydrate saturation determined based on the pressure-holding coring method.

clay sediments, respectively. c is the empirical coefficient. For Tertiary strata and more recent strata, c can be taken as 3.7 (Nie et al., 2017; Wang et al., 2017). In addition, there are other methods for calculating the relative clay content based on the natural gamma response. Because natural gamma rays are absorbed by the formation as they pass through the formation, its absorption capacity mainly depends on the formation density. Therefore, when considering the absorption of natural gamma rays by the formation, the density log response and the natural gamma log response can be combined to calculate V_c to reduce the difference in the natural gamma values caused by the different formation absorptions (Yong and Zhang, 2007):

$$V_c = \frac{GR\rho_b - GR_{ma}\rho_{ma}}{GR_c\rho_c - GR_{ma}\rho_{ma}} \tag{3}$$

where ρ_b is the density of the formation, ρ_c is the clay density, GR_{ma} is the natural gamma value of the skeleton, and ρ_{ma} is the density of the skeleton. In fact, formations all contain a certain amount of clay, and pure sandy sediments are rare. From this, a new expression of the clay content index can be obtained (Yong and Zhang, 2007):

$$I_c = \frac{GR\rho_b - GR_{min}\rho_{ma}}{GR_{max}\rho_c - GR_{min}\rho_{ma}} \tag{4}$$

Among them, it is now generally accepted that the relationship between the variation in GR and clay content is not linear, and empirical Eq. (5) is given. Eq. (2) is likewise derived empirically. The actual relationship between I_c and V_c is:

$$V_c = \frac{2^{cI_c} - 1}{2^c - 1} \tag{5}$$

In fact, the distribution of shale will also affect the response of the natural gamma log. Therefore, the above formula is only theoretical, and its evaluation effects are different for different types of reservoirs.

The inversion method of formation mineral composition based on multiple logging curves is another method for calculating clay content (Zhu et al., 2018; Liu et al., 2021; Szabó et al., 2022; Wang et al., 2022). Multiple components of the formation, including formation water, will have an effect on the log response, but the degree of effect is not the same (Li et al., 2022). For example, coarse-grained quartz sand has weak radioactivity, fine-grained clay has strong radioactivity, and the fluid in pores has the weakest radioactivity. The radioactivity of the entire natural gamma log comes from the radioactivity of the quartz, clay, and fluid. Based on this theory, Eq. (6) can be given:

$$\begin{cases} GR = V_cGR_c + V_sGR_s + \varphi GR_\varphi \\ \Delta t = V_c\Delta t_c + V_s\Delta t_s + \varphi\Delta t_\varphi \\ \rho = V_c\rho_c + V_s\rho_s + \varphi\rho_\varphi \\ \varphi_N = V_c\varphi_{Nc} + V_s\varphi_{Ns} + \varphi^*\varphi_{N\varphi} \end{cases} \tag{6}$$

where φ is the porosity, V is the volume, V_s is the sand volume fraction, Δt is the acoustic travel time, acoustic log response, ρ is the density, density log response, and φ_N is the neutron porosity log response. The subscript sand refers to the physical response and volume of the sandy part, and the subscript shale refers to the physical response and volume of the muddy part. These methods were applied at well W8, in a hydrate reservoir with deep-sea sedimentary characteristics.

3.2. Porosity

The importance of accurate porosity calculations for exploration and development is evident. Porosity calculation based on logging has always been a very reliable method. Among all conventional logging curves, density logging, neutron logging, and sonic logging are the most common logging curves used to calculate porosity. NMR logging directly measures the seepage volume characteristics of free fluids (oil, gas, and water) in arbitrary lithological reservoirs, which has obvious advantages and is widely respected (Feng et al., 2021).

The core porosity measurement of hydrate reservoirs is not as common as that of conventional oil and gas reservoirs, and core porosity data of well W8 have not yet been published publicly. Therefore, the principles of different logging curves were compared and verified. Before that, the principles of different methods were discussion.

NMR logging is a method of measuring rocks (Feng et al., 2020). It measures the paramagnetism of atomic nuclei and the external magnetic field that interacts with them. In the absence of any external magnetic field, the nuclear magnetic moment (M) of the nuclei is distributed irregularly. Under the influence of a fixed, uniform and strong magnetic field σ_0, this spin system is polarized, that is, M rearranges and aligns along the direction of the magnetic field. In a polarized magnetic field, if an alternating magnetic field is added and its frequency is also the precession frequency of protons (hydrogen nuclei), resonance absorption will occur. That is, the nuclear magnetic moment in the low-energy state shifts to the high-energy state by absorbing the energy provided by the alternating magnetic field. This phenomenon is called NMR. The numerical values of the NMR effect of various nuclei in rock-forming elements are different. The NMR value is first determined by the gyromagnetic ratio of the nuclei, the natural content of the elements in the rock and the occurrence state of the material containing the elements.

Hydrogen nuclei have the largest gyromagnetic ratio and the highest resonance frequency in the geomagnetic field. According to the gyromagnetic ratio, natural content and occurrence state of hydrogen-containing substances, hydrogen is the easiest element to study under drilling conditions. Therefore, the hydrogen nuclei contained in a certain area (from water, oil or natural gas) are the research objects of NMR logging. Organic matter and hydrates in pores cannot be measured by NMR logging (Ge et al., 2018). Therefore, the porosity obtained by NMR logging (essentially by estimating the hydrogen index) is only the fluid-filled porosity.

Both density logging and neutron porosity logging are classified as nuclear logging series. Density logging is a logging method that back-calculates the density through the absorption of γ rays by the formation. Porosity can be calculated with a sandstone volume model that uses density logging data. The neutron porosity logging data are used to back-calculate the porosity from the deceleration capacity of fast neutrons. Both instruments were calibrated in pure limestone. Similarly, sonic logging is based on the inverse calculation of porosity based on the deceleration capacity of porous rocks for acoustic waves. The traditional coarse-grained rock porosity calculation method based on the volume model is given below. The formula of the sandstone volume model that uses density logging data to calculate rock porosity is:

$$\varphi_D = \frac{\rho_{ma} - \rho_b}{\rho_{ma} - \rho_\varphi} \tag{7}$$

where φ_D is the density porosity and ρ_φ is the density of the fluids in the pore space. The formula for calculating the actual porosity of the rock from the neutron porosity is:

$$\varphi_N = \frac{\varphi_N - \varphi_{Nma}}{\varphi_{N\varphi} - \varphi_{Nma}} \tag{8}$$

where φ_N is the neutron porosity, φ_{Nma} is the neutron porosity of the skeleton, and $\varphi_{N\varphi}$ is the neutron porosity of the fluids. For the most basic formula for calculating rock porosity using sonic logging, its form is slightly different:

$$\varphi_s = \frac{\Delta t - \Delta t_{ma}}{\Delta t_\varphi - \Delta t_{ma}} \frac{1}{C_p} \tag{9}$$

where Δt is the acoustic travel time, Δt_{ma} is the acoustic travel time of the skeleton, Δt_φ is the acoustic travel time of the fluids in the pore space, and C_p is the compaction correction coefficient. The volume model is only applicable to rocks with good compaction and cementation. However, none of the above models consider the influence of shale content. The volume models of shaly sandstone and pure sandstone have different assumptions (Fig. 2).

After considering the mud content, Eqs. (7)-(9) can be rewritten as:

$$\varphi_D = \frac{\rho_{ma} - \rho_b}{\rho_{ma} - \rho_\varphi} - V_c \frac{\rho_{ma} - \rho_c}{\rho_{ma} - \rho_\varphi} \tag{11}$$

$$\varphi_N = \frac{\varphi_N - \varphi_{Nma}}{\varphi_{N\varphi} - \varphi_{Nma}} - V_c \frac{\varphi_{Nma} - \varphi_{Nc}}{\varphi_{Nma} - \varphi_{N\varphi}} \tag{12}$$

$$\varphi_s = \frac{\Delta t - \Delta t_{ma}}{\Delta t_\varphi - \Delta t_{ma}} \frac{1}{C_p} - V_c \frac{\Delta t_{ma} - \Delta t_c}{\Delta t_{ma} - \Delta t_\varphi} \tag{13}$$

To avoid errors in calculating porosity from multiple porosity logging curves, multiple porosity results are usually combined to calculate the final porosity value:

$$\varphi = \frac{\sqrt[2]{\varphi_D^2 + \varphi_N^2}}{2} \tag{14}$$

$$\varphi = \frac{\sqrt[2]{\varphi_D^2 + \varphi_N^2 + \varphi_s^2}}{3} \tag{15}$$

Porosity can also be obtained based on multicurve inversion, but the corresponding model is still a volume model, so it is not described separately here.

3.3. Water saturation

The calculation of saturation parameters is the focus of this article, and it is also the focus of a number of researchers engaged in hydrate evaluation research. The relationship between saturation and rock response is nonlinear, and it is closely related to the three-dimensional structure of the porous rock, which is why it is not easy to calculate. The Archie formula is the most common model used to calculate hydrate saturation. This may be because it is simpler and easier to determine parameters with the Archie formula than to implement rock electrical experiments. However, the requirements for the Archie formula does not match the characteristics of hydrate reservoirs. After all, the shale content in hydrate reservoirs is very high, even higher than that of shaly sandstone, and Archie's formula was based on pure sandstone. In addition, the hydrocarbons in hydrate reservoirs are not oil and gas, and their distribution in the pores is more complicated. The Archie formula can be divided into the first formula and the second formula. The corresponding standard expressions are:

$$R_o = \frac{aR_w}{\varphi^m} \tag{16}$$

$$S_w = \left(\frac{b\,R_o}{R_t}\right)^{\frac{1}{n}} \tag{17}$$

In the formula, R_o is the water-saturated rock resistivity, R_w is the formation water resistivity, R_t is the actual rock resistivity, m and n are the cementation index and saturation index, respectively, and a and b are coefficients, which can be taken as 1. Current research shows that the cementation index had the greatest influence on the calculation of water saturation, followed by the saturation index. However, as many as dozens of saturation models have been proposed, so other types of saturation models should be evaluated.

The saturation calculation model will change according to the clay content. Assuming that the clay is distributed in layers, according to the concept of parallel resistance, the layered muddy sandstone can be represented by a volume model, as shown in Fig. 3(a), and the equivalent circuit is shown in Fig. 3(b) (Poupon et al., 1954). Assuming that the resistivities of shaly sandstone, shale and pure sandstone are R_t, R_c, and R_{sd}, respectively, then:

$$\frac{V}{R_t} = \frac{V_1}{R_c} + \frac{V_2}{R_{sd}} \tag{18}$$

In the formula, V_T, V_1 and V_2 are the equivalent volumes of shaly, argillaceous and pure sandstones, respectively. Combined with Archie formula theory for further model derivation:

$$S_w^n = \frac{aR_w}{(1 - V_c)\left(\frac{\varphi}{1 - V_c}\right)^m}\left(\frac{1}{R_t} - \frac{V_c}{R_c}\right) \tag{19}$$

When the clay is dispersed, it fills the pore space between the

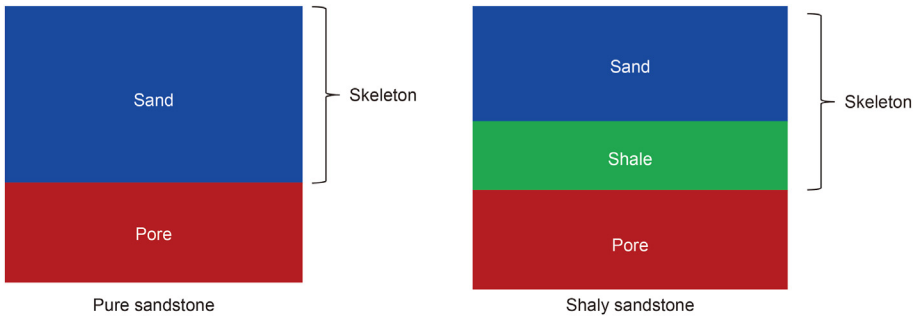

Fig. 2. The hypothetical difference between the volume models of shaly sandstone and pure sandstone. In shaly sandstone, the skeleton is composed of clay and sand, and it is assumed that they can not affect each other.

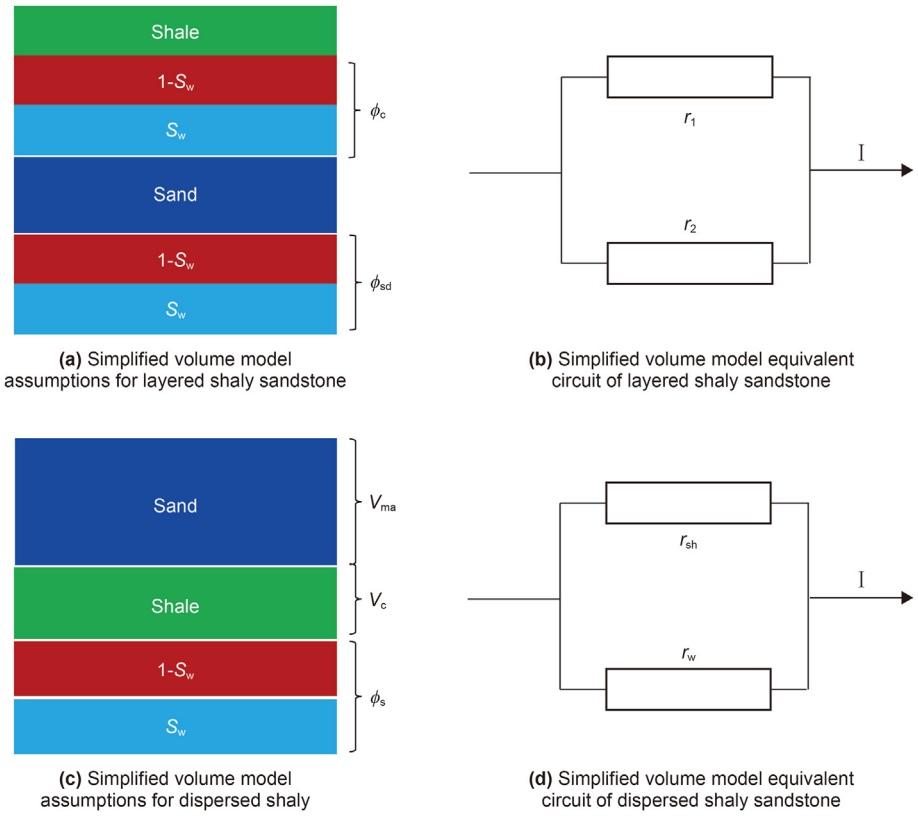

(a) Simplified volume model assumptions for layered shaly sandstone

(b) Simplified volume model equivalent circuit of layered shaly sandstone

(c) Simplified volume model assumptions for dispersed shaly

(d) Simplified volume model equivalent circuit of dispersed shaly sandstone

Fig. 3. Simplified volume model and equivalent circuit display of layered muddy sandstone, in which various elements are set in parallel, but their elements are not the same.

sand particles. The formation conductivity is the result of the parallel conduction of the formation water in the pores and the dispersed clay. The corresponding equivalent circuit is shown in Fig. 3(d). After a series of derivations, the calculation formula of S_w can be obtained as (Dewitte, 1950):

$$S_w = \sqrt{\frac{R_w\left(1-\frac{\varphi_s-\varphi_D}{\varphi_s}\right)^{mm-2}}{R_t\varphi^{mm}} + \left(\frac{(R_w-R_c)V_c}{2R_c\varphi}\right)^2} - \frac{V_c(R_c+R_w)}{2R_c\varphi} \tag{20}$$

In this formula, mm is a constant. In addition, sandstones containing mixed distribution forms of clay can be evaluated using equations such as the Simandoux equation. The corresponding formula is:

$$\frac{1}{R_t} = \frac{S_w V_c}{R_c} - \frac{\varphi^{mx} S_w^2}{R_w} \tag{21}$$

In this formula, mx is a constant. Models similar to the Simandoux equation include the Nigeria formula and the Indonesian formula.

In addition to shale content, hydrate reservoirs have both complex pore structures and complex hydrate distributions (Cai et al., 2019). Corresponding targeted models can also be tested. In this study, for the trapezoidal pore saturation model for the complex pore structure proposed by Hu et al. (2017), the corresponding derivation process is omitted, and the final saturation formula is:

$$\frac{R_t}{R_w} = \frac{\tau}{\varphi}\left(\frac{1}{P_w(S_w - f_s) + g f_s}\right) \tag{22}$$

In the formula, τ is the conductivity tortuosity, P_w is the average trapezoidal factor of the trapezoidal pores when the reservoir contains oil and gas or hydrate, f_s is the ratio of formation resistivity to formation water resistivity when the reservoir contains oil and gas, and g is the shale factor.

Considering that although the current conductivity model based on hydrate morphology has been proposed and developed rapidly, it is still difficult to directly apply it to logging evaluation, so this type of model was not used here. The selection of evaluation parameters and evaluation effects of all models for reservoirs can be seen in section 4 of the article.

4. Discussion of results

4.1. Modelling and accuracy

4.1.1. Clay content

Statistical methods, relative value methods and optimization methods were used to obtain the clay content. The relative value method adopts Eqs. (1)-(5), and the optimization method was implemented with the help of Ciflog logging software. The formula group is shown in Eq. (6).

For statistical methods, the logging curve response values of the expansion section should not be used for modelling. According to the core and logging data, this study found that the relationship between the natural gamma log response and the clay content was strong, as shown in Fig. 4. This relationship can be used to evaluate the clay content of the reservoir.

In addition, Eq. (2) and Eq. (5) were used to calculate the clay content. The core data used to determine the parameters in the model of well W8 are shown in Table 1.

For the Ciflog-based inversion algorithms, their default inversion parameters were selected without changing them. The

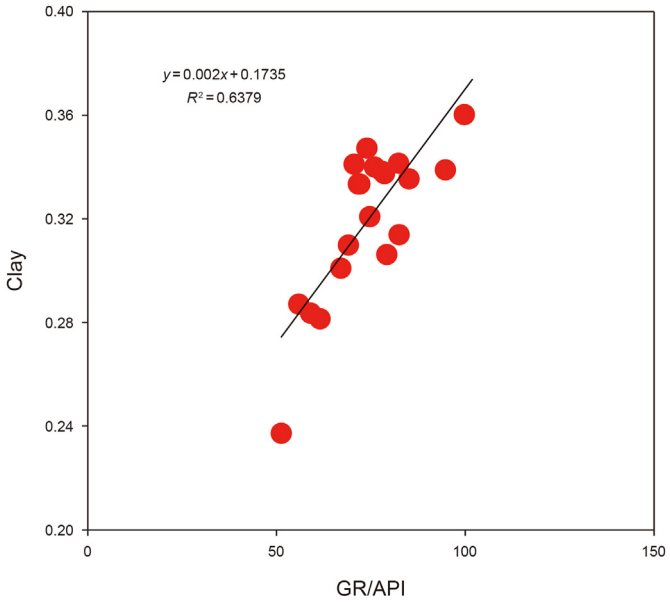

Fig. 4. Correlation between natural gamma logging data and clay content (deleted point processing).

Table 1
Determination of the parameters in the formula used to calculate the clay content.

GR_{max}	φ_c	GR_{min}	ρ_{ma}	c
155	2.2	20	2.47	3.7

corresponding results of the logging evaluation of clay content based on multiple methods are shown in Fig. 5.

Fig. 5 shows a comparison of the four tested clay content calculation methods. There were certain differences in the variation range of the curves calculated by different methods. The curve of the clay content calculation result based on the fitting method had the smallest change in the vertical direction. The natural gamma log response range of the statistical model was very small. That is, the clay content calculation results of the natural gamma logging curves in other response ranges were not necessarily accurate. The clay content calculation based on the relative value method was obviously low, and the range of clay content was large. This showed that the relative value method is not suitable for calculating the clay content of hydrate reservoirs, which are quite different from diagenetic oil and gas reservoirs.

At approximately 113.75 mbsf, it can be observed that the curve calculated by the relative value method had a good match with the core data, but in the range of 50–65 mbsf, the calculation result was significantly different from the core data. In other words, the model overestimates the impact of changes in the natural gamma logging data on the clay content of the reservoir. For deeper sediments, the radioactivity of the formation was generally higher. Compared with the results of the other two methods, the prediction result of the clay content curve based on the optimization inversion was more reliable. First, the prediction accuracy of clay content based on this method was high. Second, the clay content and particle size had a significant influence on the enrichment of hydrates, and the effect at 122.4–128.75 mbsf was observed. The apparent increase in the resistivity log response value indicated that the layer contains hydrates, but the clay content calculated by the statistical method here did not significantly decrease. Only the clay content calculated by the optimized inversion method was significantly reduced here. Therefore, after comprehensive analysis, it was suggested that for hydrate reservoirs, the clay content should be calculated using the optimized inversion method. Fig. 6 shows the comparison between the statistical method and the optimized inversion method for calculating the clay content.

Along the entire well section (20–174 mbsf), the clay content of well W8 ranged from 10.86 to 52.25%, and the average clay content was 32.35%. This shows that the overall clay content of the hydrate formation was very high. Generally, the clay content of sandstone and carbonate reservoirs does not exceed 30%, while shale is known for its high clay content, and the average clay content was approximately 35% here. Therefore, hydrate reservoirs with deep-sea sedimentary characteristics have high fine-grained clay contents, similar to shale. The optimization inversion method has also been widely used in the calculation of the clay content of shale reservoirs. Does this mean that only using natural gamma logging data to calculate the clay content of fine-grained reservoirs is not reliable enough? There was not enough evidence to determine this. Statistics show that the clay content was 28.9%. Thus, the clay content controls the amount of hydrate formation, and a slightly lower clay content will result in a large change in the amount of hydrate formation. The accurate calculation of the clay content must be considered.

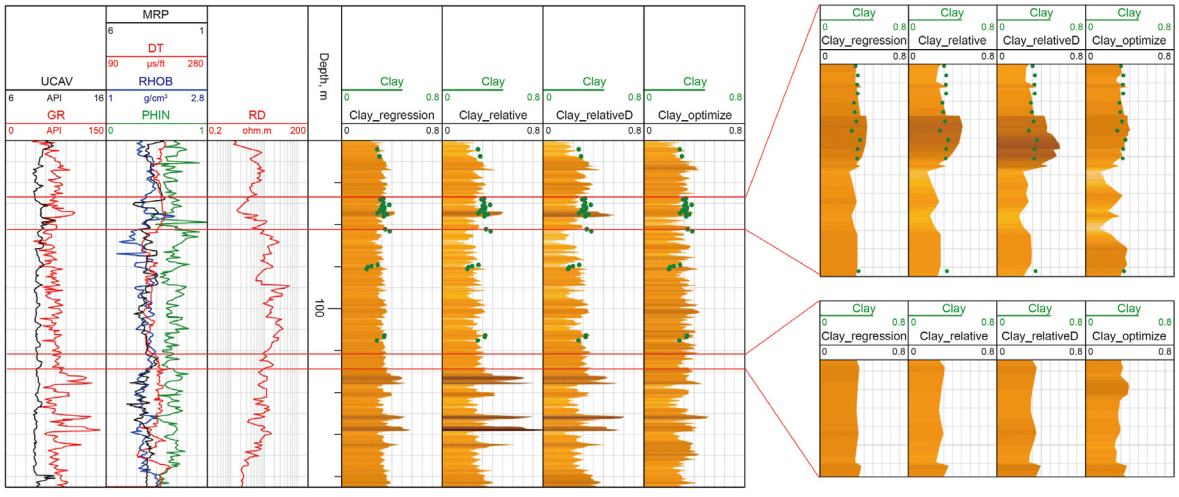

Fig. 5. Calculation results of the clay content in well W8.

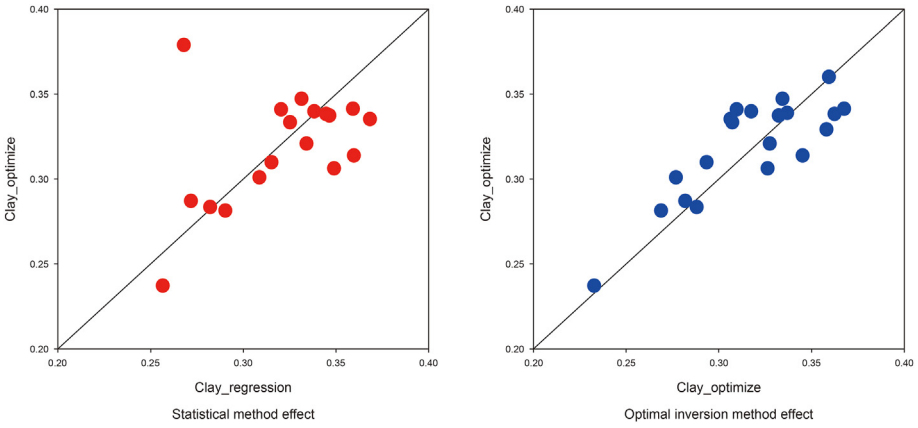

Fig. 6. Demonstration of calculation effect of clay content in W8 well.

4.1.2. Porosity

Eqs. (7)-(15) were used to evaluate the development of well W8, and the results of parameter selection in the corresponding model are shown in Table 2.

Fig. 7 shows the log calculation results of the porosity of well W8 based on the volume model.

Multiple porosity curves were used to verify the preferred method for determining the reliability of porosity calculations in this study when the core porosity was not known. The echo spacing of NMR logging is selected as 0.8 ms, and the waiting time is selected as 4 ms. Because the relaxation time of hydrate is very short (0.01 ms), it is difficult to measure the signal of hydrate under this standard, and the corresponding determined NMR porosity only contains the part without hydrate. The porosity calculated based on conventional logging can reflect the total porosity of the reservoir. In formations without hydrate, the porosity calculated by conventional logging should be consistent with the porosity calculated by NMR logging.

First, the porosity calculation results of the model considering the clay content were compared with the porosity calculation results of the conventional model. After considering the influence of clay, the porosity calculation results based on density, neutron porosity, and sonic logging curves all dropped, and the porosity drop was approximately 8%.

The water analysis data were combined to discuss the reliability of the two calculation methods. For the depth section less than 0–40 mbsf, salinity was near the baseline, but at depths below 40 mbsf, salinity was not neutralized, indicating that the change in salinity in the study area was mainly related to the formation of hydrates. That is, the hydrate content in the depth section less than 0–40 mbsf was very low, and the hydrate reservoir NMR logging porosity measured in this section should be consistent with the range of conventional logging-calculated porosity. Fig. 7 also shows the difference between the NMR logging porosity response and the conventional logging porosity response. This figure shows that the clay content must be considered in the calculation of porosity to obtain more reliable porosity calculation results.

There were also differences in the formation porosity calculated with porosity logging curves based on different principles. The porosity calculated based on sonic logging was close to the NMR logging porosity when the depth was close to 0–40 mbsf. At depths greater than 40 mbsf, the porosity calculated from NMR logging data was very close to that calculated from sonic logging data, but a large amount of hydrate occurred in the depth range of 40–174 mbsf, which was not in agreement with the actual situation. Therefore, the porosity calculated based on sonic logging data was actually low. Density logging and neutron logging data were more reliable for calculating porosity. In the 150–154 mbsf interval, the response of the resistivity logging was significantly reduced, indicating that the hydrate was not enriched in this area, and the corresponding density logging porosity was similar to the NMR logging porosity value, indicating that the density logging reliably describes the hydrate reservoir. In the 110–122 mbsf interval, the response of the resistivity logging was relatively high, indicating that the hydrate was relatively enriched here, and the porosity values calculated from neutron porosity logging and nuclear NMR logging data were different. The neutron porosity was approximately 11% larger, indicating that the neutron porosity log calculation was reliable there. Therefore, the porosity calculated by density logging and neutron porosity logging should be considered. Eq. (14) may be more suitable for calculating the porosity of well W8.

After determining the best porosity logging calculation method, the porosity range of well W8 was determined, and the average porosity was 0.514, with an interval of 0.313–0.7. This porosity range was very large. Compared with other types of reservoirs, This is one of the reasons why accurately calculating the reserves of hydrate reservoirs is more difficult than accurately calculating the reserves of other types of reservoirs.

Table 2
Determination of parameters in the formula used to calculate porosity.

ρ_{ma}	ρ_c	ρ_f
2.65	2.2	1
φ_{Nma}	φ_{Nc}	φ_{Nf}
−0.02	0.32	1
Δt_{ma}	Δt_c	Δt_f
55.5	90	189

4.1.3. Saturation

Eqs. (16)-(22), a total of 5 saturation models, were combined with porosity logging curves to calculate the water saturation of the reservoir. Since no coexistence of free gas and hydrate was observed in well W8 in the QDN area, the hydrate saturation was determined after calculating the formation water saturation. See Table 3 for all requirements and parameters of Eqs. (16)-(22).

Fig. 8 shows the saturation calculation results of the five methods and the final saturation curve. First, the most intuitive observation was that all five saturation models calculate a certain degree of hydrate saturation in the layer with a higher resistivity.

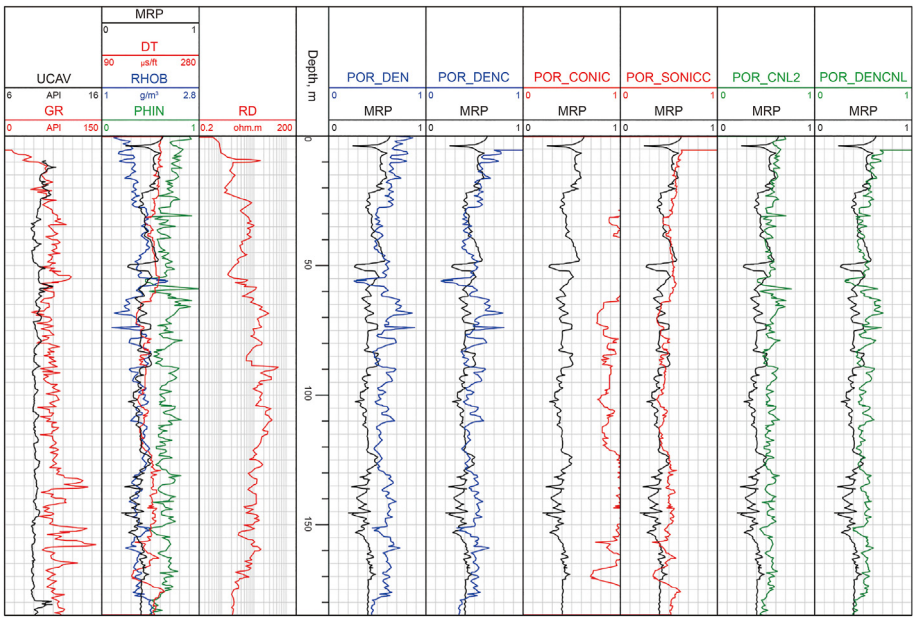

Fig. 7. Porosity calculation results for well W8.

Table 3
Parameters used in the formula to calculate the saturation.

R_w	m	n	R_c	m_2	n_2
0.22	3.642	3	2	4	4
m_3	n_3	m_4	g	f_s	P_w
5.1	3	1	1.35	0.25	0.7

However, the vertical changes in hydrate saturation calculated by the five saturation models were very different. This was caused by the multiparameter influence of the saturation model and the nonlinear model form. The saturation evaluation result based on the Archie formula had the largest value change in the longitudinal direction. This enables the model to reflect the sudden change in saturation in the formation within a certain depth. However, more often, the Archie formula overestimates hydrate saturation. For the 88–150 mbsf depth section, although the resistivity was high, the saturation was obviously not high, and the saturation value of the core was approximately 30%. Although the reason was not clarified through a series of petrophysical experiments, it was certain that

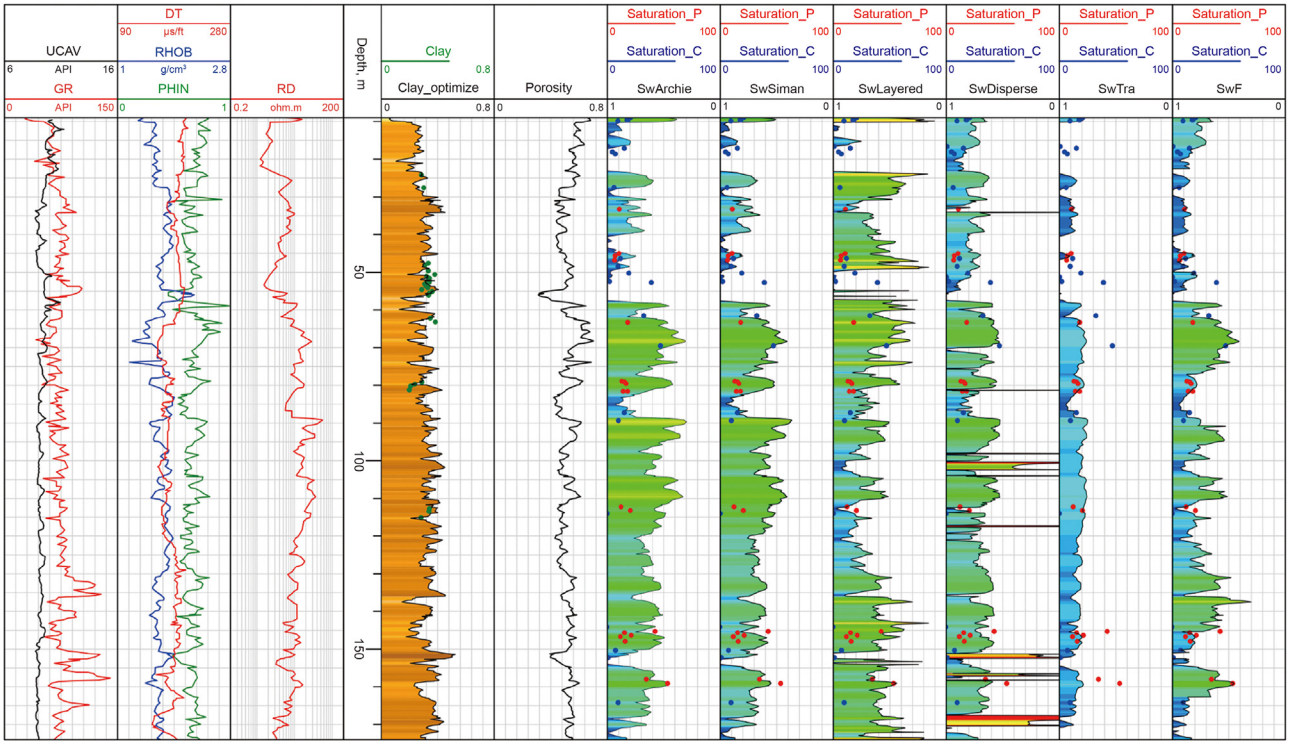

Fig. 8. Demonstration of the saturation calculation results of well W8.

the commonly used Archie formula was not reliable enough to calculate the saturation.

The calculation result of the Simandoux formula considering the influence of clay was similar to that of the Archie formula, but there were still differences. Generally, the saturation value calculated by the Simandoux formula was slightly lower than that of the Archie formula, and it can be seen that the porosity's ability to determine the saturation was reduced, and the increase in saturation in some high-porosity intervals was not as obvious as that determined with the Archie formula. The core saturation results suggested that the saturation calculated after considering the clay content was more reliable. The calculation results of the two types of saturation models considering layered clay and dispersed clay were very different. For layered clay, the calculated hydrate saturation was not high in the interval with relatively high resistivity. Interestingly, this was very consistent with the core results. With dispersed clay, the saturation values of the high-resistivity layer (such as 87–123 mbsf) and the low-resistivity layer (such as 120–150 mbsf) were similar. This seems to be more in agreement with the core results. The calculation results of three saturation models considering the distribution of different clays revealed that the hydrate reservoir of well W8 must contain a variety of different clay distribution patterns; the saturation calculation accuracy was affected when the clay distribution patterns of different intervals were not clear.

The model considering the pore structure achieved accurate calculation results for low-saturation core (Cai et al., 2019). For a long time, the pore structure of sediments was simplified so that, in many cases, the parameters of the formation factors affected by the pore structure can be directly considered as fixed values or a relationship with can be established in terms of depth to consider the impact of compaction. From this result, the generation of low hydrate saturation can be judged as probably due to the complexity of the pore structure, and the generation of high saturation was related to the improvement in the pore structure of the formation.

Then, the curve results calculated by the 5 models were combined to obtain a more reliable saturation calculation result. The principle of curve splicing is to compare the calculated saturation results with the core saturation results in a certain depth section and select the most accurate saturation model prediction result curve. The reason for this is that some of the more complex theoretical models of conductivity are more suitable for hydrate reservoirs than Archie's formula. It can be proven that the conductivity control factors of reservoirs at different depths are definitely different. The corresponding results are shown in the last section of Fig. 8. Compared with the prediction result of the Archie formula, the prediction effect of the final model was more accurate, and the trends of the prediction result curve of the Archie formula and the final model curve were different. This reflects the importance of saturation evaluation. Currently, the determination of the overall well saturation distribution mainly relies on logging methods. The use of different saturation models leads to differences in the interpretations of hydrate reservoirs. Combining the saturation evaluation results of the above five models, it can be clearly recognized that when performing reservoir evaluation and geological evaluation, the evaluation results of saturation logging without specific evaluation studies cannot be directly used as the actual saturation of the reservoir. Classification based on reservoir characteristics and modelling separately can provide reliable saturation prediction results (Zhou et al., 2019), but this is not common in hydrate reservoir log prediction.

4.2. Comprehensive reservoir classification of well W8

After obtaining the result curve, considering only the degree of enrichment of hydrates, according to the resource calculation method based on the volumetric method, the calculation formula of unit resources (ResU) is given:

$$\mathrm{ResU} = \varphi^*(1 - S_w) \tag{23}$$

Unit resource refers to the volume ratio of hydrate in a unit volume of rock. Combining this curve, the calculated dominant reservoir is shown in Fig. 9. The selected 5 layers of the dominant reservoir are obviously different from the other layers, and the unit resources are larger.

The parameter statistics of the corresponding 5 layers are shown in Table 4.

Combining Fig. 9 and Table 4, three points can be clarified through analysis. First, via the determination of highly enriched hydrate layers, it was recommended that a more accurate evaluation of some parameters should be considered in the reservoir evaluation process to assist in obtaining more accurate final results. The current evaluation of hydrate reservoirs places too much emphasis on the evaluation of saturation parameters and neglects that the formation of the reservoir should be regarded as a system. A variety of reservoir parameters jointly determine the quality of the reservoir. In this article, calculation methods and the calculation significance of clay content are shown. Fig. 9 shows that clay content was a very effective parameter for identifying high-quality reservoirs. When the clay content was low, hydrates were more likely to be enriched. The clay content curve can guide the division of layers, and the clay content curve can also help improve the accuracy of saturation evaluation. Similar information that can help the division of reservoirs may include pore structure and hydrate distribution characteristics.

Second, it was found that compared with the original log response characteristics, the reservoir parameter curve more easily summarizes the changes of the reservoir and can give better results for reservoir division. Generally, characteristics such as high resistivity and low sonic time difference are used to find hydrate-enriched layers. Based on the results of this article, it can be suggested that although this method was simple to use, the resulting curve was not effective for reservoir division. This emphasizes the importance of studying exclusively logging-based reservoir parameter models. Finally, for well W8, when the clay content was less than 0.35, the porosity was greater than 0.53, and the water saturation was less than 0.66, and the corresponding layer should be a hydrate-rich layer.

5. Development

The model application and result analysis in this study showed that the currently used hydrate logging evaluation methods were still difficult to adapt to the hydrate reservoir evaluation of well W8 in the study area. There may be three aspects that need to be further developed to improve hydrate logging evaluation:

(1) The relationships among the lithology, physical properties, hydrate properties, and electrical properties of hydrate reservoirs were not clear enough. In oil and gas reservoirs, the lithology, physical properties, oil and gas properties, electrical properties and the relationships among them are first determined during comprehensive logging evaluation. In hydrate reservoirs, these characteristics are more complicated. For example, regarding lithology, although there have been some very good studies, the quantitative influence of clay content or particle size on hydrate enrichment is still not fully understood. The hydrate reservoirs in China, India, New Zealand and other countries have fine grain sizes and high clay contents. If the lithology of the hydrate reservoir is

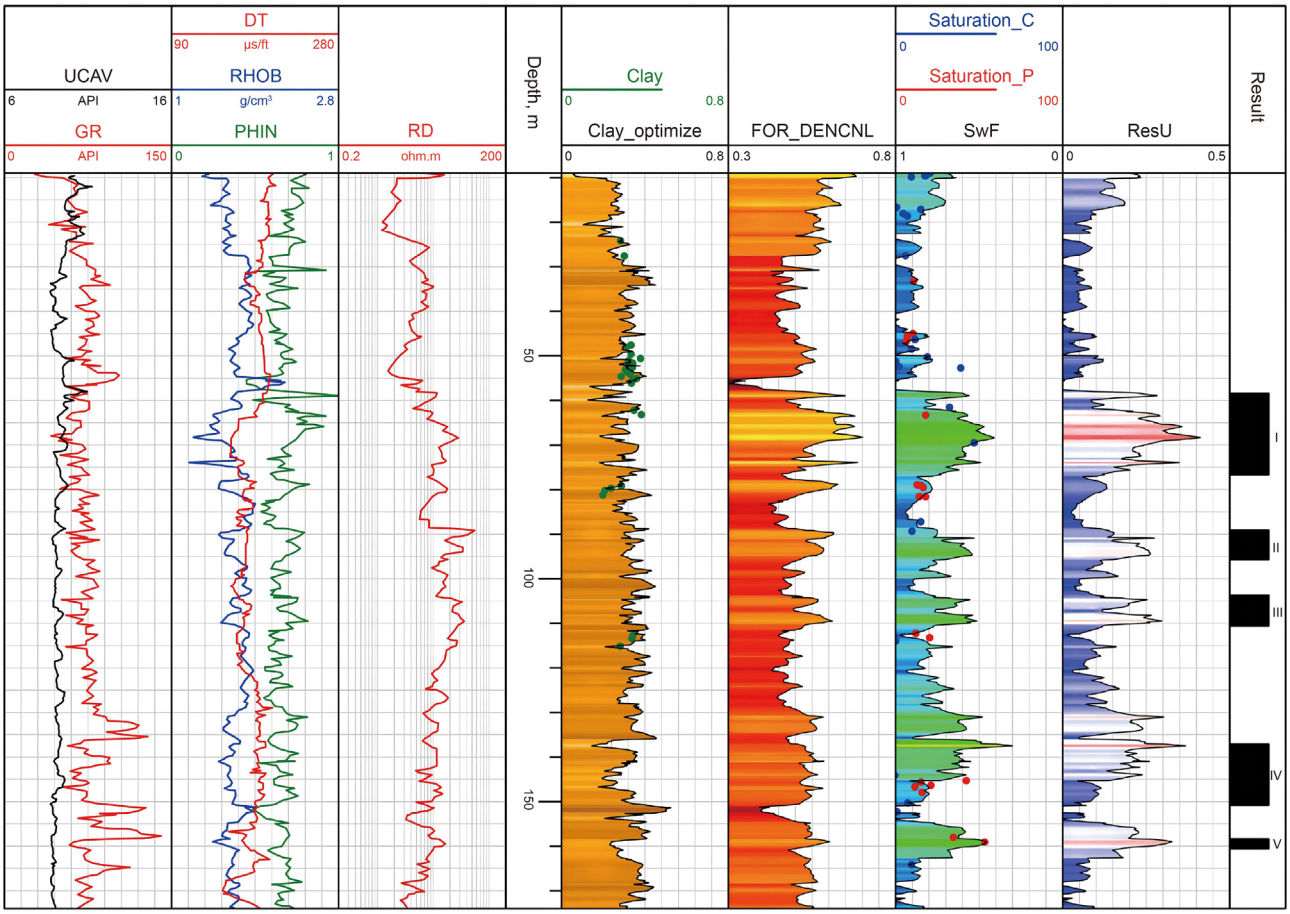

Fig. 9. Comprehensive reservoir classification results of well W8.

Table 4
Log response of all hydrate-rich layers.

Layer	GR	PHIN	RHOB	DT	RD	Clay	POR	S_w
I	65.59	0.72	1.58	171.10	12.95	0.29	0.57	0.60
II	66.41	0.73	1.61	175.08	27.66	0.33	0.57	0.65
III	69.70	0.71	1.66	173.88	25.78	0.35	0.54	0.66
IV	73.36	0.66	1.64	190.26	9.95	0.29	0.53	0.62
V	65.87	0.66	1.56	173.67	13.60	0.27	0.56	0.52

clarified, it will be of great help to identify the variation in reservoir quality. As another example, the degree of influence of porosity on the enrichment of hydrates is still unknown. To form a hydrate reservoir, what is the lower limit of porosity? In addition, based on the particularity of the hydrate distribution, what is the difference in physical response between porous hydrate reservoirs and seepage hydrate reservoirs? There have been some related studies, but an appropriate logging-based reservoir evaluation method has not yet been established, and further investment is needed to strengthen this research.

(2) The development of specialized petrophysical models for hydrate reservoirs needs to be improved. In this work, a large number of models, including the Archie formula, have been applied, but the prediction accuracy is not completely satisfactory, especially regarding the saturation. This is related to the issue that there is no currently available petrophysical model suitable for logging data. Of course, basic petrophysical research on hydrate rocks has been ongoing for a long time, and many helpful results have been obtained. However, due to the difficulty of experiments, the study of reservoir petrophysics based on core drilling and logging-based reservoir parameter evaluation is insufficient. This makes it difficult to establish a targeted quantitative model of reservoir parameters, or the model is too general to be used for logging evaluation. Reservoir petrophysics should still be the key development direction in the future.

(3) Research on hydrate reservoir evaluation based on specialized logging data is still insufficient. Electrical imaging logging can image borehole walls based on conductivity signals. Element logging can provide formation element information to invert formation mineralogy, and the mineral composition of the formation can be related to permeability. In addition, NMR logging and array acoustic logging can provide more detailed formation information. Unfortunately, a specialized logging interpretation method for hydrate reservoirs has not yet been obtained. Therefore, we have no way to directly interpret the pore structure of the formation through NMR logging, and it is also difficult to use electrical imaging logging to quantitatively characterize the fracture characteristics and hydrate distribution characteristics of leaky hydrates. Without these parameters, we would not be able to combine more formation information to calculate more accurate reservoir parameters and perform more reliable reservoir classification, such as in oil and gas reservoir logging evaluation. It is believed that follow-up research will

make the abovementioned problems easier to solve so that we can better understand hydrate reservoirs at the log scale.

6. Conclusions

In this study, using logging data and core data from well W8 in the QDN area, the clay content, porosity, and saturation of marine hydrate reservoirs with deep-sea fine-grained sedimentary characteristics were calculated, and through the calculation results, the development direction of logging evaluations of hydrate reservoirs was discussed. The study produced the following conclusions:

(1) The calculation of reservoir parameters such as porosity and saturation need to consider the influence of clay content, and the high clay content of fine-grained hydrate reservoirs causes the log response to be greatly affected. Further research on this point can improve the effectiveness of logging evaluation.
(2) The clay content calculation method based on the optimization inversion was the best for QDN well W8, and a statistical model may not be reliable enough. Without available core porosity data, the porosity of the reservoir can be evaluated by referring to the NMR porosity logging curve. It was suggested that the final porosity curve should be obtained by combining density and neutron porosity.
(3) Although a high resistivity indicated the presence of hydrate in the reservoir, the hydrate saturation was not directly proportional to the resistivity due to the complexity of the reservoir. It is difficult to use only one saturation model to accurately evaluate a reservoir. The difference in saturations calculated by different saturation models will be very large and will even affect the identification of the hydrate-enriched layer. In future reservoir saturation evaluations, determining the main controlling factors of reservoir conductivity may be a key consideration.

Declaration of competing interest

The authors declare that they have no known competing financial interests or personal relationships that could influence the work reported in this paper.

Acknowledgements

This study was funded by the Laboratory for Marine Geology, Qingdao National Laboratory for Marine Science and Technology (No. MGQNLM-KF202004); Hainan Provincial Natural Science Foundation of China (Nos. 422RC746 and 421QN281); the National Natural Science Foundation of China (No. 42106213); the China Postdoctoral Science Foundation (Nos. 2021M690161 and 2021T140691); and the Postdoctorate Funded Project in Hainan Province. The authors are grateful to the anonymous reviewers for their constructive advice on how to improve the paper.

Nomenclature

GR	natural gamma-ray log response value
GR_{min}	natural gamma-ray log values of pure sandy sediments
GR_{max}	natural gamma-ray log values of pure clay sediments
GR_s	sand natural gamma-ray log values
GR_c	clay natural gamma-ray log values
GR_φ	natural gamma-ray logging response values for fluids in the pore space
I_c	natural gamma-ray log index
V_c	clay volume fraction
V_s	sand volume fraction
ρ_b	bulk density
ρ_c	clay density
ρ_φ	fluid density in the pore space
GR_{ma}	natural gamma-ray log value of skeleton
ρ_{ma}	skeleton density
φ	porosity
V	volume
φ_D	density porosity
φ_N	neutron porosity
φ_S	sonic porosity
ρ_f	fluid density
ρ	density
φ_{Nma}	neutron porosity of skeleton
φ_{Ns}	neutron porosity of sand
φ_{Nc}	neutron porosity of clay
$\varphi_{N\varphi}$	neutron porosity for fluids in the pore space
Δt	acoustic travel time
Δt_{ma}	acoustic travel time of skeleton
C_p	compaction correction coefficient
v_{ma}	sonic velocity of skeleton
v_f	sonic velocity fluid
Δt_c	acoustic travel time of clay
Δt_s	acoustic travel time of sand
Δt_φ	acoustic travel time for fluids in the pore space
m	cementation index
n	saturation index
R_t	actual rock resistivity
R_w	formation water resistivity
R_o	water-saturated rock resistivity
R_c	clay resistivity
R_{sd}	pure sandstone resistivity
V_1	argillaceous volume
V_2	pure sandstone volume
S_w	water saturation
τ	tortuosity
P_w	average trapezoidal factor of the trapezoidal pores
f_s	ratio of formation resistivity to formation water resistivity when the reservoir contains oil and gas

References

Cai, J., Xia, Y., Lu, C., H, B., Zou, S., 2020. Creeping microstructure and fractal permeability model of natural gas hydrate reservoir. Mar. Petrol. Geol. 115, 104282. https://doi.org/10.1016/j.marpetgeo.2020.104282.

Cai, J., Zhang, Z., Wei, W., Guo, D., Li, S., Zhao, P., 2019. The critical factors for permeability-formation factor relation in reservoir rocks: pore-throat ratio, tortuosity and connectivity. Energy 188, 116051. https://doi.org/10.1016/j.energy.2019.116051.

Cheng, Y., Zhang, C., Zhu, L., 2017. A fractal irreducible water saturation model for capillary tubes and its application in tight gas reservoir. J. Pet. Sci. Eng. 159, 731–739. https://doi.org/10.1016/j.petrol.2017.09.079.

Collett, T.S., 1993. Natural gas hydrates of the prudhoe bay and kuparuk river area, north slope, Alaska. AAPG (Am. Assoc. Pet. Geol.) Bull. 77, 793–812. https://doi.org/10.1306/bdff8d62-1718-11d7-8645000102c1865d.

Collett, T.S., Lewis, R.E., Winters, W.J., Lee, M.W., Rose, K.K., Boswell, R.M., 2011. Amount of gas hydrate estimated from rock physics analysis based on morphology and intrinsic anisotropy in area B, Krishna Godavari offshore basin, expedition NGHP-02. Mar. Petrol. Geol. 28 (2), 561–577. https://doi.org/10.1016/j.marpetgeo.2020.104856.

Cook, A., Paganoni, M., Clennell, M.B., McNamara, D.D., Nole, M., Wang, X., Han, S., Bell, R.E., Solomon, E.A., Saffer, D.M., Barnes, P.M., Pecher, I.A., Wallace, L.M., LeVay, L.J., Petronotis, K.E., 2020. Physical properties and gas hydrate at a near-seafloor Thrust Fault, Hikurangi Margin, New Zealand. Geophys. Res. Lett. 47, e2020GL088474. https://doi.org/10.1029/2020gl088474.

Dewitte, L., 1950. Relation between resistivities and fluid contentd of porous rock. Oil Gas J. 49 (16), 120–132.

Fang, Y., Wei, J., Lu, H., Liang, J., Lu, J., Fu, J., Cao, J., 2019. Chemical and structural characteristics of gas hydrates from the Haima cold seeps in the Qiongdongnan Basin of the South China Sea. J. Asian Earth Sci. 182, 103924. https://doi.org/

10.1016/j.jseaes.2019.103924.
Feng, C., Feng, J., Feng, Z., Zhong, Y., Mao, Z., Ling, K., 2021. Determination of reservoir wettability based on resistivity index prediction from core and log data. J. Pet. Sci. Eng. 205, 108842. https://doi.org/10.1016/j.petrol.2021.108842.
Feng, C., Yang, Z., Feng, Z., Zhong, Y., Ling, K., 2020. A novel method to estimate resistivity index of tight sandstone reservoirs using nuclear magnetic resonance logs. J. Nat. Gas Sci. Eng. 79, 103358. https://doi.org/10.1016/j.jngse.2020.103358.
Ge, X., Liu, J., Fan, Y., Xing, D., Deng, S., Cai, J., 2018. Laboratory investigation into the formation and dissociation process of gas hydrate by Low-Field NMR technique. J. Geophys. Res. Solid Earth 123 (5), 3339–3346. https://doi.org/10.1029/2017jb014705.
Ge, X., Fan, Y., Liu, J., Zhang, L., Han, Y., Xing, D., 2017a. An improved method for permeability estimation of the bioclastic limestone reservoir based on NMR data. J. Magn. Reson. 283, 96–109. https://doi.org/10.1016/j.jmr.2017.09.004.
Ge, X., Fan, Y., Xiao, Y., Liu, J., Xing, D., Gu, D., Deng, S., 2017b. Quantitative evaluation of the heterogeneity for tight sand based on the nuclear magnetic resonance imaging. J. Nat. Gas Sci. Eng. 38, 74–80. https://doi.org/10.1016/j.jngse.2016.12.037.
Ghosh, R., Ojha, M., 2021. Amount of gas hydrate estimated from rock physics analysis based on morphology and intrinsic anisotropy in area B, Krishna Godavari offshore basin, expedition NGHP-02. Mar. Petrol. Geol. 124, 104856. https://doi.org/10.1016/j.marpetgeo.2020.104856.
Gullapalli, S., Dewangan, P., Dakara, G., Mishra, C.K., 2019. Seismic evidence of free gas migration through the gas hydrate stability zone (GHSZ) and active methane seep in Krishna-Godavari offshore basin. Mar. Petrol. Geol. 110, 695–705. https://doi.org/10.1016/j.marpetgeo.2019.07.052.
Han, S., Bangs, N.L., Hornbach, M.J., Pecher, I.A., Tobin, H.J., Silver, E.A., 2021. The many double BSRs across the northern Hikurangi margin and their implications for subduction processes. Earth Planet. Sci. 558, 116743. https://doi.org/10.1016/j.epsl.2021.116743.
Horozal, S., Bahk, J., Urgeles, R., Kim, G.Y., Cukur, D., Kim, S.P., Lee, G.H., Lee, S.H., Ryu, B., Ki, J., 2017. Mapping gas hydrate and fluid flow indicators and modeling gas hydrate stability zone (GHSZ) in the Ulleung Basin, East (Japan) Sea: potential linkage between the occurrence of mass failures and gas hydrate dissociation. Mar. Petrol. Geol. 80, 171–191. https://doi.org/10.1016/j.marpetgeo.2016.12.001.
Hu, S., Zhou, C., Li, X., Li, C., Zhang, S., 2017. A tight sandstone trapezoidal pore oil saturation model. Petrol. Explor. Dev. 44 (5), 876–886. https://doi.org/10.1016/s1876-3804(17)30099-x.
Hu, Y., Xie, J., Xue, S., Xu, M., Fu, C., He, H., Liu, Z., Ma, S., Sun, S., Wang, C., 2021. Research and application of thermal insulation effect of natural gas hydrate freezing corer based on the wireline-coring principle. Petrol. Sci. https://doi.org/10.1016/j.petsci.2021.11.019. Available online.
Jain, V., Saumya, S., Vij, J., Singh, J., Singh, B., Pattnaik, S., Oli, A., Kumar, P., Collett, T.S., 2019. New technique for accurate porosity estimation from logging-while-drilling nuclear magnetic resonance data, NGHP-02 expedition, offshore, India. Mar. Petrol. Geol. 108, 570–580. https://doi.org/10.1016/j.marpetgeo.2018.11.001.
Jang, J., Cao, S.C., Stern, L.A., Waite, W.F., Jung, J., Lee, J.Y., 2020. Potential freshening impacts on fines migration and pore-throat clogging during gas hydrate production: 2-D micromodel study with Diatomaceous UBGH2 sediments. Mar. Petrol. Geol. 80, 171–191. https://doi.org/10.1016/j.marpetgeo.2020.104244.
Kato, A., Konno, Y., Yoneda, J., Kida, M., Oshima, M., Jin, Y., Nagao, J., Tenma, N., 2019. Evaluation of failure modes and undrained shear strength by cone penetrometer for Natural Gas hydrate-bearing pressure-core sediment samples recovered from the Krishna–Godavari Basin, offshore India. Mar. Petrol. Geol. 108, 502–511. https://doi.org/10.1016/j.marpetgeo.2018.11.015.
Kret, K., Tsuji, T., Chhun, C., Takano, O., 2020. Distributions of gas hydrate and free gas accumulations associated with upward fluid flow in the Sanriku-Oki forearc basin, northeast Japan. Mar. Petrol. Geol. 116, 104305. https://doi.org/10.1016/j.marpetgeo.2020.104305.
Larinonv, V.V., 1969. Radiometry of Boreholes (In Russian). Nedra, Moscow. https://doi.org/10.4236/ojps.2021.112016.
Li, B., Nie, X., Cai, J., Zhou, X., Wang, C., Han, D., 2022. U-Net model for multi-component digital rock modeling of shales based on CT and QEMSCAN images. J. Pet. Sci. Eng. 216, 110734. https://doi.org/10.1016/j.petrol.2022.110734.
Li, Y., Liu, L., Jin, Y., Wu, N., 2021. Characterization and development of natural gas hydrate in marine clayey-silt reservoirs: a review and discussion. Adv. Geo-Energy Res. 5 (1), 75–86. https://doi.org/10.46690/ager.2021.01.08.
Liang, J., Zhang, W., Lu, J., Wei, J., Kuang, Z., He, Y., 2019. Geological occurrence and accumulation mechanism of natural gas hydrates in the eastern Qiongdongnan Basin of the South China Sea: insights from site GMGS5-W9-2018. Mar. Geol. 418, 106042. https://doi.org/10.1016/j.margeo.2019.106042.
Lin, Y., Liu, Y., Xu, K., Li, T., Zhang, Z., Wu, J., 2022. Strengthening and weakening of methane hydrate by water vacancies. Adv. Geo-Energy Res. 6 (1), 23–37. https://doi.org/10.46690/ager.2022.01.03.
Liu, L., Zhang, Z., Li, C., Ning, F., Liu, C., Wu, N., Cai, J., 2020. Hydrate growth in quartzitic sands and implication of pore fractal characteristics to hydraulic, mechanical, and electrical properties of hydrate-bearing sediments. J. Nat. Gas Sci. Eng. 75, 103109. https://doi.org/10.1016/j.jngse.2019.103109.
Liu, W., Zhang, C., Zhang, Z., Li, J., Zhu, L., Hu, S., Zhou, X., 2021. A new method of mineral inversion based on error analysis and static response equation error: a case study of a shale gas reservoir in the Wufeng-Longmaxi Formation. Interpretation 10, 1–10. https://doi.org/10.1190/INT-2019-0208.1.
Meng, M., Liang, J., Lu, J., Zhang, W., Kuang, Z., Fang, Y., He, Y., Deng, W., Huang, W., 2021. Quaternary deep-water sedimentary characteristics and their relationship with the gas hydrate accumulations in the Qiongdongnan Basin, Northwest South China Sea. Deep-Sea Res., Part A I 418, 106042. https://doi.org/10.1016/j.dsr.2021.103628.
Nie, X., Wan, Y., Bie, F., 2017. Dual-shale-content method for total organic carbon content evaluation from wireline logs in organic shale. Open Geosci. 9 (1), 133–137. https://doi.org/10.1515/geo-2017-0011.
Pandey, L., Sian, K., Joshi, A.K., 2019. Estimate of gas hydrate saturations in the Krishna-Godavari basin, eastern continental margin of India, results of expedition NGHP-02. Mar. Petrol. Geol. 108, 581–594. https://doi.org/10.1016/j.marpetgeo.2018.12.009.
Portnov, A., Cook, A.E., Sawyer, D.E., Yang, C., Hillman, J.T., Waite, W.F., 2019. Clustered BSRs: evidence for gas hydrate-bearing turbidite complexes in folded regions, example from the Perdido Fold Belt, northern Gulf of Mexico. Earth Planet. Sci. 528, 115843. https://doi.org/10.1016/j.epsl.2019.115843.
Poupon, A., Gaymard, R., 1970. The evaluation of clay content from logs. In: SPWLA 11th Annual Logging Symposium. Society of Petrophysicists and Well-log Analysts.
Poupon, A., Loy, M.E., Tixer, M.P., 1954. A contribution to electrical log interpretation in shaly sands. J. Petrol. Technol. 6 (6), 27–34. https://doi.org/10.2118/311-G.
Qi, R., Qin, X., Cheng, L., Ma, C., Mao, W., Zhang, W., 2022. Experimental study on the isothermal adsorption of methane gas in natural gas hydrate argillaceous silt reservoir. Adv. Geo-Energy Res. 6 (2), 143–156. https://doi.org/10.1016/j.ijhydene.2019.07.090.
Qian, J., Wang, X., Collett, T.S., Guo, Y., Kang, D., Jin, J., 2018. Downhole log evidence for the coexistence of structure II gas hydrate and free gas below the bottom simulating reflector in the South China Sea. Mar. Petrol. Geol. 98, 662–674. https://doi.org/10.1016/j.marpetgeo.2018.09.024.
Qian, J., Wang, X., Dong, D., Sain, K., Ye, Y., 2019. New estimation of anisotropic saturation and fracture quantitative evaluation for fracture-filling gas hydrate reservoir. Prog. Geophys. 34 (1), 354–364. https://doi.org/10.6038/pg2019BB0569.
Saumya, S., Barasimhan, B., Singh, J., Yamamoto, H., Vij, J., Sakiyama, N., Kumar, P., 2019. Acquisition of logging-while-drilling (LWD) multipole acoustic log data during the India national gas hydrate program (NGHP) expedition 02. Mar. Petrol. Geol. 108, 562–569. https://doi.org/10.1016/j.marpetgeo.2018.10.011.
Saito, S., Hsiung, K., Sanada, Y., Moe, K., Hamada, Y., Nakamura, Y., Wu, H., Shinmoto, Y., Yamada, Y., NGHP Expedition 02 JAMSTEC Science Team, 2019. Gas hydrate occurrence and distribution controlled by regional geological structure off eastern India: estimates from logging-while-drilling in Area-B, National Gas Hydrate Program Expedition 02 (NGHP-02). Mar. Petrol. Geol. 108, 216–225. https://doi.org/10.1016/j.marpetgeo.2018.12.050.
Shankar, U., Gupta, D., Bhowmick, D., Sain, K., 2013. Gas hydrate and free gas saturations using rock physics modelling at site NGHP-01-05 and 07 in the Krishna–Godavari Basin, eastern Indian margin. J. Pet. Sci. Eng. 106, 62–70. https://doi.org/10.1016/j.petrol.2013.04.004.
Shaibu, R., Sambo, C., Guo, B., Dudun, A., 2021. An assessment of methane gas production from natural gas hydrates: challenges, technology and market outlook. Adv. Geo-Energy Res. 5 (3), 318–332. https://doi.org/10.46690/ager.2021.03.07.
Singh, A., Ojha, M., 2022. Machine learning in the classification of lithology using downhole NMR data of the NGHP-02 expedition in the Krishna-Godavari offshore Basin, India. Mar. Petrol. Geol. 135, 105443. https://doi.org/10.1016/j.marpetgeo.2021.105443.
Singh, R.P., Lall, D., Vishal, V., 2022. Prospects and challenges in unlocking natural-gas-hydrate energy in India: recent advancements. Mar. Petrol. Geol. 135, 105397. https://doi.org/10.1016/j.marpetgeo.2021.105397.
Sun, J., Dong, H., Muhammad, A., Yu, L., Zhang, Y., Golsanami, N., Yan, W., 2021. Influence of pore structural properties on gas hydrate saturation and permeability: a coupled pore-scale modelling and X-ray computed tomography method. J. Nat. Gas Sci. Eng. 88, 103805. https://doi.org/10.1016/j.jngse.2021.103805.
Szabó, N., Remeczki, F., Jobbik, A., Kiss, K., Dobróka, M., 2022. Interval inversion based well log analysis assisted by petrophysical laboratory measurements for evaluating tight gas formations in Derecske through, Pannonian basin, east Hungary. J. Pet. Sci. Eng. 208, 109607. https://doi.org/10.1016/j.petrol.2021.109607.
Waite, W.F., Ruppel, C.D., Collett, T.S., Schultheiss, P., Holland, M., Shukla, K.M., Kumar, P., 2019. Multi-measurement approach for establishing the base of gas hydrate occurrence in the Krishna-Godavari Basin for sites cored during expedition NGHP-02 in the offshore of India. Mar. Petrol. Geol. 108, 296–320. https://doi.org/10.1016/j.marpetgeo.2018.07.026.
Wang, B., Zhang, Z., Xing, L., Lao, L., Wei, Z., Ge, X., 2021b. Integrated dielectric model for unconsolidated porous media containing hydrate. J. Pet. Sci. Eng. 59 (7), 5563–5578. https://doi.org/10.1109/tgrs.2020.3017251.
Wang, H., Liu, T., Tang, T., Shi, Y., 2017. A unified model to evaluate shaliness in compacted and soft formations using downhole GR log. IEEE Trans. Geosci. Electron. 156, 877–883. https://doi.org/10.1016/j.petrol.2017.06.070.
Wang, J., Wu, S., Sun, J., Feng, W., Li, Q., 2021a. Influence of seafloor topography on gas hydrate occurrence across a submarine canyon-incised continental slope in the northern margin of the South China Sea. Mar. Petrol. Geol. 133, 105279. https://doi.org/10.1016/j.marpetgeo.2021.105279.
Wang, X., Wu, S., Lee, M., Guo, Y., Yang, S., Liang, J., 2011. Gas hydrate saturation from acoustic impedance and resistivity logs in the Shenhu area, South China

Sea. Mar. Petrol. Geol. 28 (9), 1625–1633. https://doi.org/10.1016/j.marpetgeo.2011.07.002.
Wang, Z., Nie, X., Zhang, C., Wang, M., Zhao, J., Jin, L., 2022. Lithology classification and porosity estimation of tight gas reservoirs with well logs based on an equivalent multi-component model. Front. Earth Sci. 10, 850023. https://doi.org/10.3389/feart.2022.850023.
Wei, J., Deng, Y., 2020. Deeply buried authigenic carbonates in the Qiongdongnan Basin, South China sea: implications for ancient cold seep activities. Minerals 10, 1135. https://doi.org/10.3390/min10121135.
Wei, J., Wu, T., Zhu, L., Fang, Y., Liang, J., Lu, H., Cai, W., Xie, Z., Lai, P., Cao, J., Yang, T., 2021. Mixed gas sources induced co-existence of sI and sII gas hydrates in the Qiongdongnan Basin, South China Sea. Mar. Petrol. Geol. 128, 105024. https://doi.org/10.1016/j.marpetgeo.2021.105024.
Wei, J., 2021. Physical properties of gas hydrate-bearing pressure core sediments in the South China Sea. Geofluids 6636125, 1–10. https://doi.org/10.1155/2021/6636125.
Wu, D., Peng, J., Sun, M., Gao, Q., Zhang, X., Qiang, S., Bo, K., 2016. Experimental study on a pressure-coring technology based on a freeze-core valve for marine hydrate-bearing sediment sampling. J. Nat. Gas Sci. Eng. 33, 135–142. https://doi.org/10.1016/j.jngse.2016.05.023.
Yang, L., Chen, W., Liu, W., Zha, B., Zhu, L., 2020. Random noise attenuation based on residual convolutional neural network in seismic datasets. IEEE Access 8, 30271–30286. https://doi.org/10.1109/access.2020.2972464.
Yadav, U.S., Shukla, K.M., Ojha, M., Kumar, P., Shankar, U., 2019. Assessment of gas hydrate accumulations using velocities derived from vertical seismic profiles and acoustic log data in Krishna-Godavari Basin, India. Mar. Petrol. Geol. 108, 551–561. https://doi.org/10.1016/j.marpetgeo.2019.02.001.
Ye, J., Wei, J., Liang, J., Lu, J., Lu, H., Zhang, W., 2019. Complex gas hydrate system in a gas chimney, South China Sea. Mar. Petrol. Geol. 104, 29–39. https://doi.org/10.1016/j.marpetgeo.2019.03.023.
You, J., Cao, J., Wang, X., Liu, W., 2021. Shear wave velocity prediction based on LSTM and its application for morphology identification and saturation inversion of gas hydrate. J. Pet. Sci. Eng. 205, 109027. https://doi.org/10.1016/j.petrol.2021.109027.
Yong, S., Zhang, C., 2007. Logging Data Processing and Comprehensive Interpretation. China University of Petroleum Press, Dongying, pp. 447–449.
Zhou, S., Yang, L., Xue, K., Zhao, J., Liu, Y., Yang, S., 2021. Fine sand migration in hydrate-bearing sediments and median grain size ratio optimization of gravel pack. J. Nat. Gas Sci. Eng. 88, 103809. https://doi.org/10.1016/j.jngse.2021.103809.
Zhou, X., Zhang, C., Zhang, Z., Zhang, R., Zhu, L., Zhang, C., 2019. A saturation evaluation method in tight gas sandstones based on diagenetic facies. Mar. Petrol. Geol. 107, 310–325. https://doi.org/10.1016/j.marpetgeo.2019.05.022.
Zhong, G., Zhang, D., Zhao, L., 2021. Current states of well-logging evaluation of deep-sea gas hydrate-bearing sediments by the international scientific ocean drilling (DSDP/ODP/IODP) programs. Nat. Gas. Ind. B 8 (2), 128–145. https://doi.org/10.1016/j.ngib.2020.08.001.
Zhu, L., Ma, Y., Cai, J., Zhang, C., Wu, S., Zhou, X., 2021. Key factors of marine shale conductivity in southern China—Part I: the influence factors other than porosity. J. Pet. Sci. Eng. 205, 108698. https://doi.org/10.1016/j.petrol.2021.108698.
Zhu, L., Ma, Y., Cai, J., Zhang, C., Wu, S., Zhou, X., 2022a. Key factors of marine shale conductivity in southern China—Part II: the influence of pore system and the development direction of shale gas saturation models. J. Pet. Sci. Eng. 205, 109516. https://doi.org/10.1016/j.petrol.2021.109516.
Zhu, L., Zhang, C., Guo, C., Jiao, Y., Chen, L., Zhou, X., Zhang, C., Zhang, Z., 2018. Calculating the total porosity of shale reservoirs by combining conventional logging and elemental logging to eliminate the effects of gas saturation. Petrophysics 59 (2), 162–184. https://doi.org/10.30632/PJV59N2-2018a4.
Zhu, L., Wei, J., Wu, S., Zhou, X., Sun, J., 2022b. Application of unlabelled big data and deep semi-supervised learning to significantly improve the logging interpretation accuracy for deep-sea gas hydrate-bearing sediment reservoirs. Energy Rep. 8 (1), 2947–2963. https://doi.org/10.1016/j.egyr.2022.01.139.